Electronic Supplementary Material (ESI) for Nanoscale.

Supplementary Information: Far-field Optical Nanothermometry using Individual sub-50 nm Upconverting Nanoparticles

Jacob D. Kilbane[1], Emory M. Chan[2], Christian Monachon[1,2], Nicholas J. Borys[2], Elizabeth S. Levy[2], Andrea D. Pickel[1], Jeffrey J. Urban[2], P. James Schuck[2], Chris Dames[1,2,*]

[1]Department of Mechanical Engineering, University of California, Berkeley, California 94720, United States

[2]The Molecular Foundry, Lawrence Berkeley National Laboratory, Berkeley, California 94720, United States

*cdames@berkeley.edu

Contents

(A) Sample preparation

Nanoparticles were spin coated at 2000 RPM for 3 seconds onto an optical-quality borosilicate glass coverslip (Fisherbrand™, transparent at 980 nm). The coverslip had previously been cleaned by sonication for 10 minutes each in acetone, isopropyl alcohol, and then distilled water, followed by 30 seconds of plasma cleaning.

(B) Bright field image of metal line defect region used for locating single nanoparticles

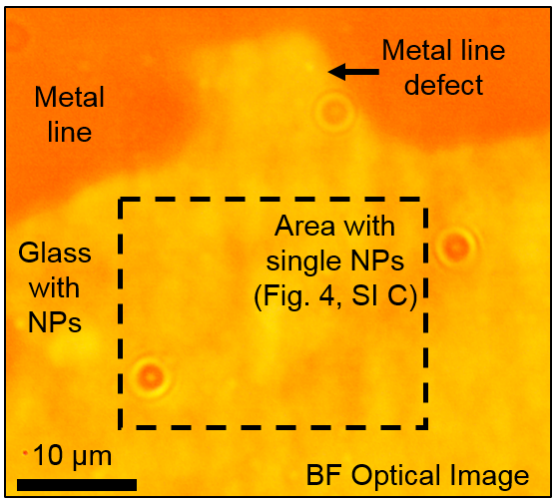

Figure S1 - Bright field optical image of the edge of a microfabricated metal line with defects, used to identify the location of imaged nanoparticles. Darker region is the shadow of the metal line and lighter region is the clear glass coverslip. Circular spots are optical artifacts. Image is blurry because the light is coming from behind, rather than front-side imaging as in Fig. 2.

(C) Particle map matching APD scans of single particles with SEM images for particles #2 and #3

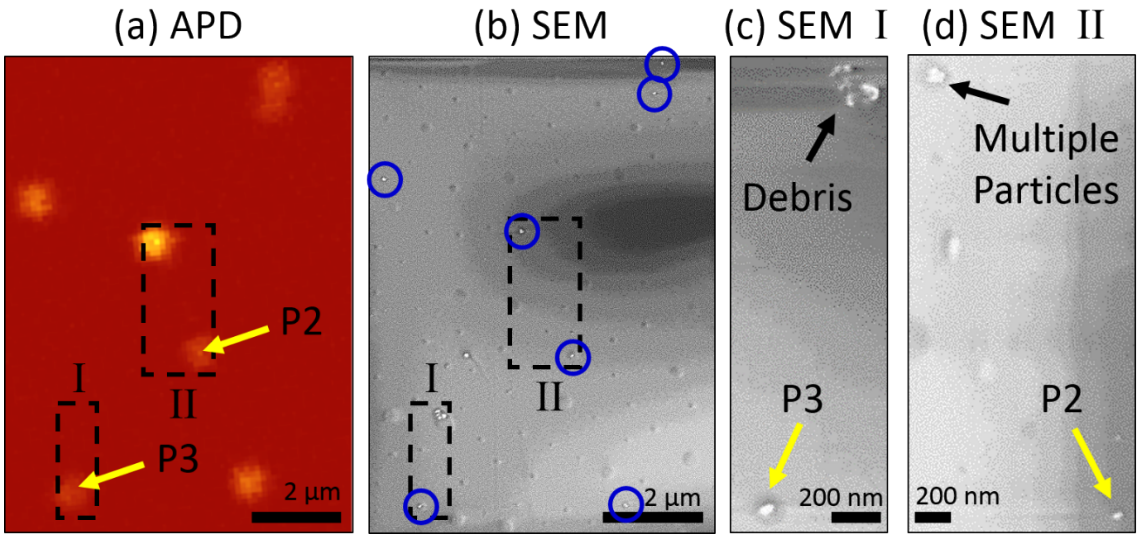

Figure S2 - Self-consistent optical and SEM identification of single particles. (a) APD image containing the single particles #2 and #3 used in Fig. 5 for thermometry. (b) SEM image corresponding to the same region as the APD (both images aligned using the unique metal feature in SI B, outside the field of view here). Particle locations are highlighted in blue circles. The SEM image also shows additional non-luminescent features, thought to be non-particle debris, dimples in the coverslip, or charging artifacts. (c)-(d) Higher resolution SEM images of the single particles, clearly identifying them as individual 20 x 40 nm nanoparticles. All SEM images were obtained by averaging as many as 50 fast scans to limit charging effects.

(D) Sensitivity of single nanoparticle temperature measurements

Sensitivity is defined as either $S = \frac{1}{R}\frac{dR}{dT}$ or $S = \frac{dR}{dT}$ for photoluminescence thermometry via lanthanide-doped nanoparticles (refs [1] and [2], respectively). Figure S3 below shows the sensitivity for both definitions, using representative values A = 5.8 and ΔE = 98.7 meV (variations of S among the five particles are not shown and are minor, since all five particles had similar values of A and ΔE). These results compare well with ensemble measurements,[3] which is expected because the relative spectra weight between the two bands λ_{1-2} and λ_{2-3} in Eq. (1) is independent of absolute luminescence intensity (i.e. A and ΔE are independent of the number of particles).

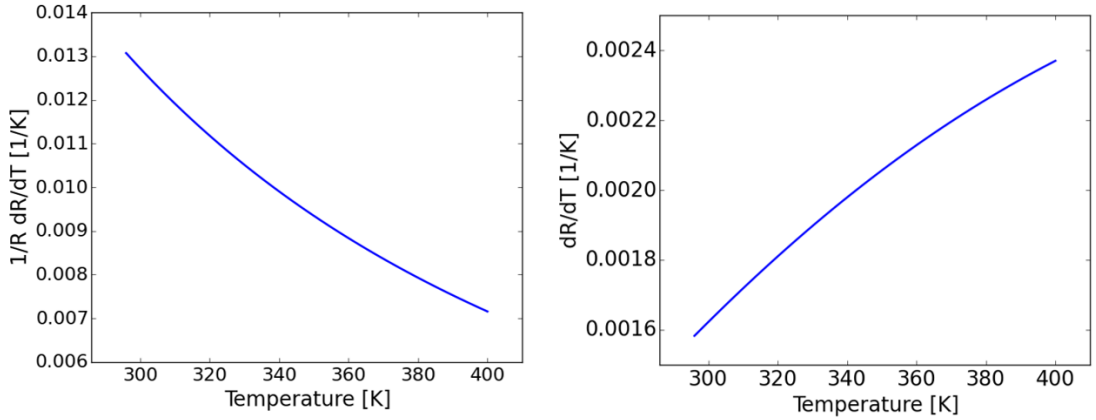

Figure S3 - Sensitivity vs. temperature, calculated using representative values for A and ΔE

(E) Detection limits and uncertainty in temperature

We assess the detection limits of this technique by considering the smallest detectable temperature change using a single, well-calibrated particle. We assess the uncertainty in temperature by considering a random particle picked from a batch pre-calibrated using the five particles in Fig. 5. Details are

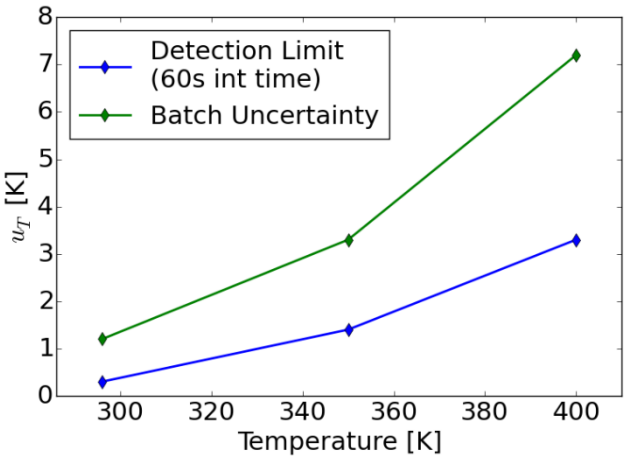

Figure S4 – Detection limit of a single well-calibrated particle (blue) and temperature uncertainty for a random particle picked from a batch calibrated using the five particles in Fig. 5 of the main text (green).

provided below with results summarized in Fig. S4.

Smallest detectable temperature change with 60 s integration time

We consider having a particular particle, which can be calibrated so the $R(T)$ function is well known. In the present context, with the model of Eq. (1) this corresponds to known A and ΔE. We ask, what is the smallest temperature change ΔT which can be reliably detected, i.e. by causing $\Delta R \geq u_R$ where u_R is the uncertainty in R?

With A and ΔE known, this detection limit is given by $\Delta T = \frac{dT}{dR} u_R$, where $\frac{dT}{dR}$ is obtained by differentiating Eq. (1) and using the average A and ΔE values from Table 1. To quantify u_R we used another single particle and took seven successive measurements (60 s integration time) each at 296 K, 350 K, and 400 K. The resulting standard deviations σ_R were 1.1%, 3.3%, and 5.2%, respectively, of their means. Using Student's t analysis to convert these σ_R to u_R (68% confidence interval), we find the detection limits to be $\Delta T \approx \pm 0.3$ K at 296 K, ± 1.4 K at 350 K, and ± 3.3 K at 400 K (68% confidence interval, seven measurements at 60 s integration time). These results are summarized in Fig. S4.

A measure of batch uncertainty

We consider a batch of particles, of which N have been carefully calibrated with functions $R_p(T)$ well known, where $p = 1 \ldots N$. In the present context, this corresponds to having N values each of A_p and ΔE_p.

The statistics of these A_p and ΔE_p thus characterize the batch. Now a new particle is drawn from the batch, but not calibrated. It is placed in an unknown environment, and we measure a value R with uncertainty u_R. We ask, what is the uncertainty u_T in the resulting temperature, considering u_R as well as the variability of batch statistics?

We use a method similar to a Monte Carlo method of error propagation[4] to quantify the uncertainty. We assess the uncertainty in T corresponding to the three R values of 0.1210, 0.2200, and 0.3310 (chosen to correspond to representative low, medium, and high temperature regimes, respectively). For example, suppose R_{meas}=0.2200 is measured. For each of the five particle's calibration curves, p=1-5, we calculate the corresponding temperature $T_p = \frac{\Delta E_p}{k_b \ln\left(A_p / R_{meas.}\right)}$ from Eq. (1). Graphically this is equivalent to finding the five intersections of the five best-fit curves and the horizontal line R_{meas}=0.2200, as depicted in Fig. S5. R_{meas} itself carries uncertainty u_R, which we take here to equal the standard deviation of the seven successive R measurements, for example u_R= 0.0069 for R around 0.22 (that is, for T around 350 K). Therefore, the $R \rightarrow T$ uncertainty propagation was repeated five more times using $R_{meas} + u_R$ = 0.2269, and another five times with $R_{meas} - u_R$ = 0.2131.

The resulting ensemble of 15 temperatures represents a population of possible temperatures if we had no knowledge of which of the five particles was actually being measured, which approximates the case for another particle drawn at random from the batch. So we finally take the standard deviation of these 15 values, which in this case is $u_T \approx$ 3.3 K for T around 350 K. Repeating this exercise at low (296 K) and high (400 K) temperatures gives $u_T \approx$ 1.2 K and $u_T \approx$ 7.2 K, respectively. These results are summarized in Fig. S4.

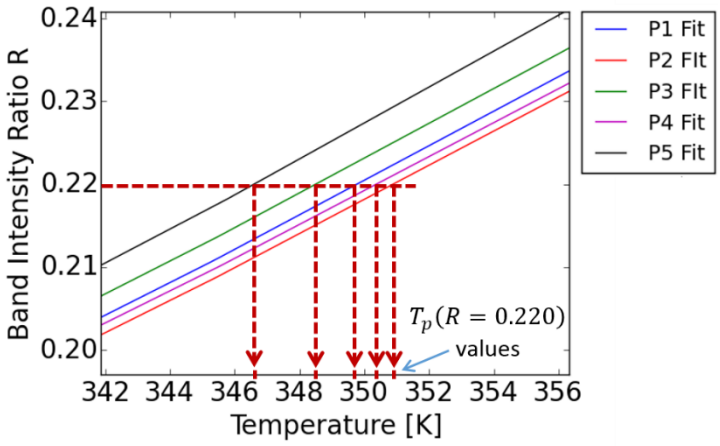

Figure S5 - Visual representation of our approach to quantifying the batch uncertainty, shown here for R = 0.22. Without knowing which particle p was measured, a measured intensity ratio, R_{meas}=0.22, could correspond to any of the five depicted temperatures T_p, indcated by the five vertical lines. (Fit curves are extracted directly from Fig. 5 of the main text.)

(F) Noise floor estimates

A change in temperature associated with a change in R is:

$\Delta T = \frac{dT}{dR}\Delta R$,

where $\frac{dT}{dR}$ comes from Eq. (1). Similarly, if we have a noisy signal, the equivalent temperature from noise σ_R is:

$\sigma_T = \frac{dT}{dR}\sigma_R$.

Using the definition as given by ref,[5] the noise floor can be estimated as:

$\eta_T \equiv \sigma_T\sqrt{t_{integration}}$.

Using the standard deviations of seven successive measurements at 296 K, 350 K, and 400 K to define σ_R (σ_R/R = 1.1%, 3.3%, and 5.2%, respectively), the representative values A=5.7 and ΔE=98.7 meV, and $t_{integration}$= 60s, we calculate noise floors of $\eta_T =$ 6 $K/\sqrt{Hz}$, 26 $K/\sqrt{Hz}$, and 63 $K/\sqrt{Hz}$, respectively.

(G) Optical saturation data

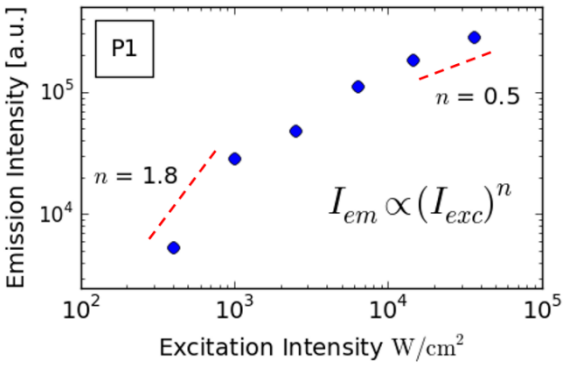

Figure S6 - Emission intensity vs. excitation intensity plot showing that we were operating near the saturated regime (temperature data in the main text Fig. 5 taken at 2×10^4 W/cm^2), because increases in excitation intensity provide weaker than a quadratic increase in emission intensity.[6] Emission intensity is the integrated photon counts (through 550 ± 20 nm BP filter) over an APD scan of particle #1, after subtracting the background from an equivalent APD scan with the laser blocked.

(H) Calculations showing self-heating of nanoparticle due to absorption is negligible

We believe self-heating of these particles is negligible based on the following calculations. Light at 980 nm is primarily absorbed by the Yb^{3+} ions,[6–8] with an effective absorption cross section of order 10^{-24} m^2.[7,9,10] Given that the atomic density of Yb^{3+} ions at 20% is 2.7 ions/nm^3 [6] and our particles are around 20 x 20 x 40 nm^3 in volume, the total heat absorbed at 10^5 W/cm^2 excitation density is q_{abs} = 40 pW. Considering that the contact area and contact resistance of the particle on the surface is unknown, a conservative estimate of the temperature rise can be found by completely neglecting all heat transfer into the substrate, instead considering only the heat loss by conduction to air. The relevant thermal model is the solution for a sphere embedded in an infinite medium, which gives the temperature rise as $\Delta T = q_{abs}/(4\pi k_{eff} r)$ where r is the particle radius and k_{eff} is the effective conductivity of the surrounding air, which will be less than handbook values due to rarefied gas effects. This effective air thermal conductivity can be estimated based on kinetic theory using $k_{eff} = C\bar{v}\Lambda/3$ where the mean free path Λ (approximately 68 nm at 300 K for air) is replaced by the radius of the particle, conservatively assumed to be 20 nm. Using $C = 1000$ J/m^3K for the specific heat at constant pressure and $\bar{v} = \sqrt{8RT/\pi} = 470$ m/s for $R = 287$ J/kg-K and T = 300 K, the effective air thermal conductivity is approximately 0.003 W/m-K. An alternative estimate of k_{eff} for a similar embedded sphere geometry using the Boltzmann transport equation solution for phonon thermal conductivity where phonon mean free path is replaced with molecular mean free path (68 nm) provides the same effective air conductivity value of 0.003 W/m-K.[11] Finally, if we further assume only the upper half of the particle can lose heat to the air, the temperature rise due to absorption acquires an additional factor of two. At an excitation density of 10^5 W/cm^2, the resulting (conservative) temperature rise estimate is 0.2 K, which is negligible for this work.

References

1. Zhou, S. *et al.* Upconversion luminescence of NaYF4: Yb3+, Er3+ for temperature sensing. *Opt. Commun.* **291,** 138–142 (2013). doi:10.1016/j.optcom.2012.11.005

2. Li, D., Shao, Q., Dong, Y. & Jiang, J. Thermal sensitivity and stability of NaYF4:Yb3+, Er3+ upconversion nanowires, nanorods and nanoplates. *Mater. Lett.* **110,** 233–236 (2013). doi:10.1016/j.matlet.2013.08.047

3. Vetrone, F. *et al.* Temperature sensing using fluorescent nanothermometers. *ACS Nano* **4,** 3254–8 (2010). doi:10.1021/nn100244a

4. Press, W., Teukolsky, S., VetterlingW & Flannery, B. *Numerical Recipes: The Art of Scientific Computing, 3rd.* (Cambridge University Press, 2007).

5. Plakhotnik, T., Aman, H. & Chang, H.-C. All-optical single-nanoparticle ratiometric thermometry with a noise floor of 0.3 K Hz −1/2. *Nanotechnology* **26,** 245501 (2015). doi:10.1088/0957-4484/26/24/245501

6. Gargas, D. J. *et al.* Engineering bright sub-10-nm upconverting nanocrystals for single-molecule imaging. *Nat. Nanotechnol.* **9,** 300–5 (2014). doi:10.1038/nnano.2014.29

7. Singh, S. K., Kumar, K. & Rai, S. B. Er3+/Yb3+ codoped Gd2O3 nano-phosphor for optical thermometry. *Sensors Actuators A Phys.* **149,** 16–20 (2009). doi:10.1016/j.sna.2008.09.019

8. Aarts, L., van der Ende, B. M. & Meijerink, A. Downconversion for solar cells in NaYF4:Er,Yb. *J. Appl. Phys.* **106,** 023522 (2009). doi:10.1063/1.3177257

9. DeLoach, L. *et al.* Evaluation of absorption and emission properties of Yb/sup 3+/ doped crystals for laser applications. *IEEE J. Quantum Electron.* **29,** 1179–1191 (1993). doi:10.1109/3.214504

10. Mialon, G. *et al.* High Up-Conversion Efficiency of YVO 4 :Yb,Er Nanoparticles in Water down to the Single-Particle Level. *J. Phys. Chem. C* **114,** 22449–22454 (2010). doi:10.1021/jp107900z

11. Chen, G. Nonlocal and Nonequilibrium Heat Conduction in the Vicinity of Nanoparticles. *J. Heat Transfer* **118,** 539 (1996). doi:10.1115/1.2822665